

Complexed crystal structure of replication restart primosome protein PriB reveals a novel single-stranded DNA-binding mode

Cheng-Yang Huang¹, Che-Hsiung Hsu^{1,2}, Yuh-Ju Sun², Huey-Nan Wu¹ and Chwan-Deng Hsiao^{1,*}

¹Institute of Molecular Biology, Academia Sinica, Taipei, 115, Taiwan and ²Institute of Bioinformatics and Structural Biology, National Tsing Hua University, Hsinchu, 300, Taiwan

Received April 28, 2006; Revised July 4, 2006; Accepted July 13, 2006

Protein Data Bank accession no. 2ccz

ABSTRACT

PriB is a primosomal protein required for replication restart in *Escherichia coli*. PriB stimulates PriA helicase activity via interaction with single-stranded DNA (ssDNA), but the molecular details of this interaction remain unclear. Here, we report the crystal structure of PriB complexed with a 15 bases oligonucleotide (dT15) at 2.7 Å resolution. PriB shares structural similarity with the *E.coli* ssDNA-binding protein (*EcoSSB*). However, the structure of the PriB–dT15 complex reveals that PriB binds ssDNA differently. Results from filter-binding assays show that PriB–ssDNA interaction is salt-sensitive and cooperative. Mutational analysis suggests that the loop L₄₅ plays an important role in ssDNA binding. Based on the crystal structure and biochemical analyses, we propose a cooperative mechanism for the binding of PriB to ssDNA and a model for the assembly of the PriA–PriB–ssDNA complex. This report presents the first structure of a replication restart primosomal protein complexed with DNA, and a novel model that explains the interactions between a dimeric oligonucleotide-binding-fold protein and ssDNA.

INTRODUCTION

The ability to restart replication after encountering DNA damage is essential for bacterial survival (1,2). The ϕ X-type primosome, or ‘replication restart’ primosome (3–5), is a protein–DNA complex that re-activates stalled DNA replication at forks after DNA damage (6). PriB is one of the *Escherichia coli* primosomal proteins. Together with PriA,

PriC, DnaT, DnaB, DnaC and DnaG, PriB is required for the assembly of the ϕ X-type primosome (7). Although the sequence of assembly during the ϕ X-type primosome formation (PriB is the second to assemble) has been well studied (3,7), the role plays by PriB is poorly understood at the molecular level. PriB can bind both ssDNA and ssRNA (8–10). It also stabilizes the binding of PriA to DNA hairpins and thereby facilitates the association of DnaT with the primosome (7). In addition, a recent study suggests that upon forming the PriA–PriB–ssDNA complex, PriB induces a conformational alteration in PriA resulting in stimulated PriA helicase activity (11).

PriB exists as a homodimer (8–10), and each polypeptide has 104 residues. The PriB monomer has an oligonucleotide/oligosaccharide-binding (OB)-fold structure with three flexible β -hairpin loops: L₁₂ (residues 20–24), L₂₃ (residues 37–44) and L₄₅ (residues 81–88). It shares structural similarity with the DNA-binding domain of *E.coli* ssDNA-binding protein (*EcoSSB*) (1,2,12). The structural resemblance suggests PriB may bind ssDNA in a manner similar to *EcoSSB*. However, several lines of evidence indicate that they have different ssDNA-binding modes. First, the amino acid sequences of PriB and *EcoSSB* share only 11% identity and 27% similarity (Figure 1A). Second, *EcoSSB* exists as homotetramer (13), while PriB is a homodimer. Third, *in vitro* assays have shown that *EcoSSB* inhibits whereas PriB stimulates PriA helicase activity (11).

In order to perceive a mechanistic model of ϕ X-type primosome assembly, it is important to elucidate the structure of the PriB–ssDNA complex and understand the ssDNA-binding properties of PriB. In this study, we present the crystal structure of PriB complexed with a 15mer oligodeoxythymidylate (dT15) at 2.7 Å resolution. This structural model is compared with that of the *EcoSSB*–ssDNA complex (13). We also conducted ssDNA-binding assays with wild-type and PriB mutants to investigate the nature of the PriB–ssDNA interaction.

*To whom correspondence should be addressed. Tel: +886 2 2788 2743; Fax: +886 2 2782 6085; Email: hsiao@gate.sinica.edu.tw

The authors wish it to be known that, in their opinion, the first two authors should be regarded as joint First Authors

© 2006 The Author(s).

This is an Open Access article distributed under the terms of the Creative Commons Attribution Non-Commercial License (<http://creativecommons.org/licenses/by-nc/2.0/uk/>) which permits unrestricted non-commercial use, distribution, and reproduction in any medium, provided the original work is properly cited.

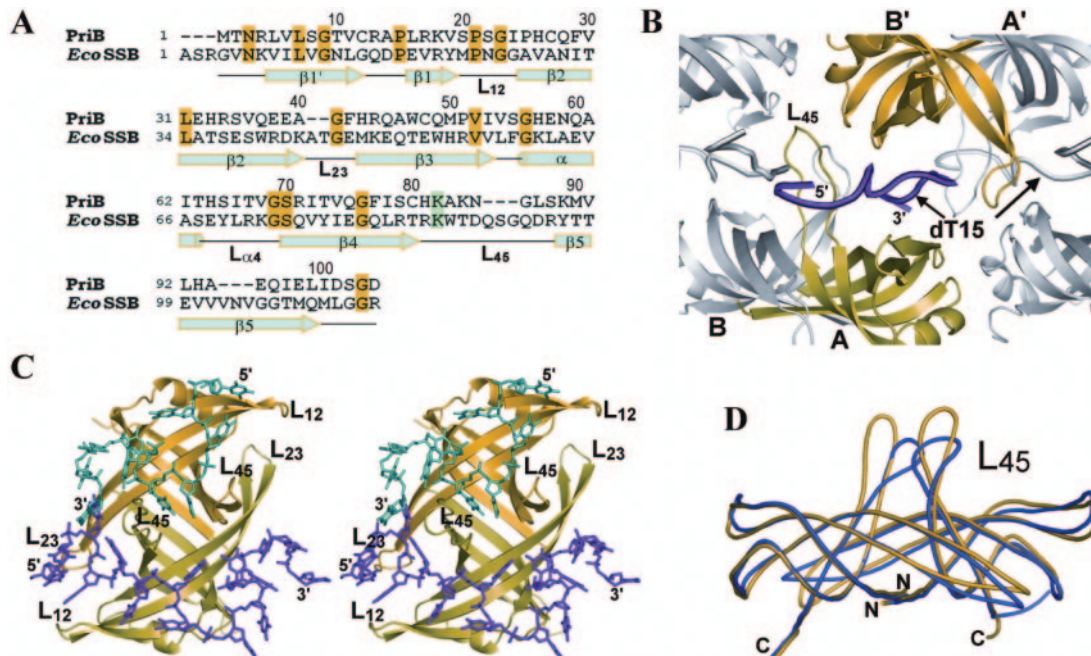


Figure 1. Structure of the PriB–dT15 complex. (A) Sequence alignment of PriB and *EcoSSB*. Identical residues between PriB and *EcoSSB* are indicated in yellow, and the conserved lysine residues (Lys82 in PriB and Lys87 in *EcoSSB*) involved in ssDNA binding are indicated in cyan. The secondary structural elements of PriB are shown below the sequences. (B) Periodic interactions between the PriB dimers and dT15 oligonucleotides in the complex crystal. An asymmetric unit contains a PriB dimer and one dT15. The dT15 (magenta trace) is sandwiched by monomer A (green ribbon) and monomer B' (yellow ribbon) from the symmetrically related dimer. For clarity, the remaining symmetrical molecules are shown in gray. (C) A stereo view of a PriB dimer interacting with two dT15 oligonucleotides. The two oligonucleotides (magenta and cyan stick models) are related by crystallographic 2_1 symmetry. (D) Structural overlay of PriB dimers in apo (blue) and dT15-bound yellow forms. The two structures are shown as C α traces, and the L₄₅ loops are labeled.

MATERIALS AND METHODS

Protein expression and purification

The encoding region of wild-type and PriB mutants were put on pET-21b expression vectors and expressed with a His₆ affinity tag at the C-terminal of the recombinant proteins. Details of the construction and protein purification have been described previously (8). The PriB mutants were generated according to the Stratagene QuickChange mutagenesis protocol (Stratagene, La Jolla, CA) using the pET21b-PriB plasmid as template (8). Based on the secondary structure measurements determined by circular dichroism spectroscopy, the mutated proteins appeared to be correctly folded. These mutants have identical chromatographic behavior as that of the wild-type PriB on a size-exclusion column (data not shown). Therefore, amino acids substituted on these mutants do not affect PriB-dimer formation under the chromatographic conditions we used.

Nucleic acids

Various lengths of ssDNA oligonucleotides were custom synthesized by MdBio, Inc. (Frederick, MD). The nucleic acid homopolymers were 5' end labeled with T4 polynucleotide kinase (Promega, Madison, WI) and [γ -³²P]ATP (6000 Ci/mmol; PerkinElmer Life Sciences).

Filter-binding assay

The affinity of PriB to ssDNA was examined by a double-filter-binding assay (14,15). Briefly, ssDNA–PriB complexes

were generated by incubating 1 nM of ³²P-labeled oligonucleotide with various concentrations of PriB (10⁻⁵ to 10⁻⁹ M) for 30 min at 25°C in a binding buffer containing 50 mM HEPES, pH 7.0, and 40 μ g/ml BSA. The reaction mixture, in a total volume of 50 μ l, was filtered through a nitrocellulose membrane overlaid on a Hybond N+ nylon membrane (Amersham Pharmacia Biotech). The membranes have been pre-soaked for 10 min in a washing buffer containing 50 mM HEPES, pH 7.0, and 10 mM NaCl, before being framed into a dot-blotting apparatus. The slots were washed immediately with 100 μ l of washing buffer before and after the sample filtering step. The radioactivity on both filters was quantified with a PhosphorImager (Molecular Dynamics), and the fraction of bound ssDNA was estimated.

Apparent dissociation constants were determined by plotting the fraction of ssDNA bound at each protein concentration and then fitting the data to the following equation: $\theta = [P]/([P] + K_d)$, in which θ is the fraction of ssDNA bound, $[P]$ is the concentration of total protein, and K_d is the apparent dissociation constant. Cooperative binding to ssDNA sites was assessed by plotting the fraction of ssDNA bound over a range of protein concentrations, and the binding data were analyzed by fitting the data to the following equation: $\log(\theta/(1 - \theta)) = h \log[P] - h \log K_d$, where h is the Hill coefficient (16).

Mobility shift assays with agarose gel electrophoresis

The affinity of PriB protein for ϕ X ssDNA was examined with a published method used for the analysis of the SSB– ϕ X

ssDNA complex (17). Briefly, PriB proteins in various concentrations as specified in the figure legends were incubated in 40 mM HEPES, pH 7.0, 80 mM NaCl and 100 nM of circular ϕ X ssDNA (Biolab) at 25°C for 30 min. Aliquots (5 μ l) were removed from each reaction solution and mixed with 1 μ l of loading dye (0.25% bromophenol blue and 40% sucrose). The samples were analyzed by electrophoresis on 0.8, 1, 2 and 3% agarose gels using a Tris–borate–EDTA buffer (45 mM Tris–borate and 1 mM EDTA, pH 8.5). Bands corresponding to unbound ϕ X ssDNA and PriB– ϕ X ssDNA complexes were visualized by ethidium bromide (0.5 μ g/ml) staining.

Crystallization and data collection

Before crystallization, PriB was concentrated to 6 mg/ml in 20 mM sodium citrate and 50 mM NaCl (pH 5.0), and ssDNA was added to a molar ratio of 1:2.5 (PriB-dimer:ssDNA). The samples were then incubated at 37°C for 30 min. Crystals of PriB–dT15 and PriB–dT30 were grown by the hanging drop vapor diffusion method at 20°C. Both complex crystals grew within 1 week after mixing 1 μ l of the protein–ssDNA complex solution with 1 μ l of reservoir solution containing 25% (w/v) PEG 3350, 50 mM Bis–Tris, pH 6.5. Both PriB–dT15 and PriB–dT30 crystals grew as clusters of thin plates with dimensions of \sim 0.3 mm \times 0.1 mm \times 0.01 mm. Parafilm oil was used as a cryoprotectant before the crystals were flash frozen. Each dataset was collected on a Rigaku R-AXIS IV++ image-plate detector (Rigaku, MSC) using a synchrotron radiation X-ray source at Beamline 17B2 of the National Synchrotron Radiation Research Center in Taiwan. Data integration and scaling were performed using the *HKL* package (18).

Structure determination and refinement

The structure of PriB bound to dT15 was solved by the molecular replacement software AMoRe (19) using DNA-unbound PriB [Protein Data Bank (PDB) accession no. 1V1Q] with its flexible L₄₅ and L₁₂ loops trimmed off. The clearest solution was found at an *R*-factor of 46% and at a correlation coefficient of 61.3%. Following molecular replacement, model building was performed using the program XtalView (20). The loops were gradually built as the quality of the map improved. After the loops were almost entirely built, electron density corresponding to DNA was observed in both σ_A -weighted $2F_o - F_c$ and $F_o - F_c$ maps (21). The DNA structure was built into a $2F_o - F_c$ electron density map 1 nt at a time to avoid preconceived notions of strand topology. Molecular dynamics refinement was performed using the program CNS (22) with a 20–2.7 Å resolution range, and 10% of the data was selected to calculate the R_{free} factor to monitor refinement. The B-factors were higher in the ssDNA (57.89 Å²) than in the protein (38.66 Å²). The final structure was refined to an *R*-factor of 25.0% and an R_{free} of 28.4%. The ligand occupancies were estimated from alternating cycles of B-factor and occupancy refinement, which resulted in a value of 0.7. Partial occupancy of ssDNA-binding sites has been observed previously. For example, occupancy of ssDNA ligand in a 2.8 Å crystal structure of *Eco*SSB is 0.67 (13). The stereochemical quality was checked by a Ramachandran plot generated using the pro-

gram PROCHECK (23). The statistics for structure refinements of the PriB–dT15 and the PriB–dT30 complexes are listed in Table 1.

Electron microscopy

Electron microscopy was used to examine the PriB–ssDNA complexes. Complexes of PriB molecules (46 μ l; 600 μ g/ml) and intact circular ϕ X ssDNA (4 μ l; 20 μ g/ml) were formed by mixing the solutions. They were then diluted directly into 0.01 M ammonium acetate (pH 7.0) and incubated for 20 min at 25°C. The complexes were adsorbed to a carbon film that had been made hydrophilic by exposure to a high-voltage glow discharge. The adsorbed complexes were exposed to 1% (w/v) aqueous uranyl acetate, dried, and then imaged with a goniometer stage in a Zeiss EM10CA electron microscope. Images on films were scanned with a Nikon LS4500 film scanner.

RESULTS

Overall structure of the PriB dimer in complex with dT15

To investigate the molecular details of the interaction between PriB and ssDNA, crystals of the PriB–dT15 and the PriB–dT30 complexes were subjected to X-ray diffraction studies. Both crystals belong to space group P2₁2₁2₁ with similar cell dimensions (Table 1); the PriB–dT15 and PriB–dT30 complexes diffracted to 2.7 and 4.5 Å resolution, respectively. Owing to the resolution limit and data quality, we focused on the PriB–dT15 complex structure in this study. The majority of the electron density for PriB and dT15 was of good quality, but a discontinuity was observed for T9 to T11 of dT15, suggesting that this region is dynamic.

Table 1. Data collection and refinement statistics

Dataset	PriB–dT15	PriB–dT30
Data collection		
Space group	P2 ₁ 2 ₁ 2 ₁	P2 ₁ 2 ₁ 2 ₁
<i>a</i> (Å)	45.54	45.92
<i>b</i> (Å)	51.15	51.36
<i>c</i> (Å)	99.10	100.46
Resolution (Å)	20–2.7	20–4.5
<i>R</i> _{sym} (%) ^a	6.9 (41.8) ^b	13.3 (65.4)
<i>I</i> / σ (<i>I</i>)	18.5 (3.6)	19.2 (4.5)
Completeness (%)	99.6 (100.0)	78.5 (66.3)
Redundancy	4.9	3.2
Refinement		
Resolution (Å)	20–2.7	
<i>R</i> / <i>R</i> _{free}	25.0/28.4	
Number of atoms		
Protein	1763	
Nucleic acid	297	
Water	119	
B-factors		
Protein	38.66	
Nucleic acid	57.89	
Water	36.69	
Root mean square deviations		
Bond lengths (Å)	0.012	
Bond angles (°)	2.000	

^a $R_{\text{merge}}(I) = \sum_i \sum_l |I_i - I| / \sum_l I$, where *I* is the mean intensity of the *i* observations of reflection *h*.

^bNumbers in parentheses are for data with a high-resolution cutoff at 2.7 Å.

Each asymmetric unit contains one PriB dimer and one dT15 oligonucleotide. Although PriB dimers made few contacts with each other, through their interaction with dT15 they packed as a thread with crystallographic 2_1 symmetry along the *b*-axis (Figure 1B). Owing to periodic interactions between PriB dimers and dT15 oligonucleotides every oligonucleotide is sandwiched by monomer A from one dimer and the adjacent monomer B' from a symmetrically related dimer. Consequently, every PriB dimer contacts two symmetrically related dT15 oligonucleotides (Figure 1C). In the complex, two ssDNA-binding surfaces from two adjacent PriB dimers confine the DNA-binding path, and the bound dT15 adopts an Ω -shaped conformation.

PriB–dT15 interactions

The occupancy of bound dT15 in the crystal is 0.7. This feature has also been found in the crystal of *Eco*SSB tetramers complexed with two oligodeoxycytidylates of 35 bases long (dC35) (13). Single-stranded DNA-binding proteins (SSBs) act as sequence-independent ssDNA chaperones. Hence, it has been suggested that SSBs do not limit the conformation of the bound ssDNA to the extent as that observed for other known DNA-binding proteins (24), so that the largely unstructured ssDNA can slide freely through the ssDNA-binding domain of SSB (25). Consequently, this high DNA mobility causes the bound DNAs to be either disordered (24) or have a low occupancy (13). Recently a genomic study indicates that PriB evolved from *Eco*SSB via gene duplication with subsequent rapid sequence divergence (26). Thus, PriB may have inherited its ssDNA-binding nature from its ancestor, *Eco*SSB.

Although PriB binds ssDNA on the surface of its OB folds as *Eco*SSB, PriB and *Eco*SSB are likely distinct in their ssDNA-binding mechanisms because of the difference in the extent of oligomerization and the conformation of the L_{23} loop. PriB forms a dimer and its L_{23} loop from each subunit makes close contact with the β -barrel core. *Eco*SSB, however, forms a tetramer, and its longer L_{23} loops protrude away from the β -barrel core in the presence or absence of ssDNA (13,27). The extended L_{23} loops greatly increase the interactions between *Eco*SSB and ssDNA. A long stretch of ssDNA wraps around the outside of the homotetramer. In contrast, owing to the closed conformation of the L_{23} loops, PriB has a relatively shallow DNA-binding surface on the two OB folds of the dimer and ssDNA wraps around the L_{45} loops (Figure 1C).

The structure of the PriB dimer in the ssDNA-bound state is mostly similar to that of the apo form without DNA, with significant conformational changes only in the L_{45} loops (Figure 1D) of the protein. In the apo form (8–10), the L_{45} loops of the PriB dimer are remarkably flexible. However, both L_{45} loops are stabilized by interacting strongly with the ssDNA in the PriB–dT15 complex. The L_{45} loop in PriB is shorter than that in *Eco*SSB and has different protein–protein interacting abilities. One of the two stabilized L_{45} loops contacts another L_{45} loop in a symmetry related dimer (Figure 1B). The contact surface area between PriB dimers is small ($\sim 288 \text{ \AA}^2$). Apparently the thread-like ultrastructure of the PriB dimer found in the crystal is mainly credited to the association of PriB to ssDNA. In *Eco*SSB,

the L_{45} loops are probably important for the continuous assembly of homotetramers that wrap the ssDNA. They pair intermolecularly via antiparallel β -sheets and bring the tetramers together in the crystals of both the apo (27) and the ssDNA-complexed forms (13).

Since PriB dimers and dT15 oligonucleotides interact periodically in the crystal, for clarity, we will mainly address the interactions among monomer A, dT15, and the adjacent monomer B' from the symmetry related dimer (Figure 1B). Usually, an OB fold interacts with only a certain span of ssDNA (28). As shown in Figure 2A, a single dT15 oligonucleotide interacts with two OB folds from two symmetry related PriB dimers. The 5' and 3' termini of dT15 interact mainly with monomer A, while the central region of dT15 makes many contacts with monomer B'. The dT15 adopt an Ω -shaped conformation to accommodate the two ssDNA-binding surfaces. We postulate that dT15 primarily binds to monomer A, but the central region of dT15 is partially dissociated from monomer A due to competitive binding for monomer B'. This competition between monomer A and B' yields a variety of conformers that are relatively isoenergetic, resulting in weaker electron density in the central region of the dT15 compares with that at the two ends.

In the *Eco*SSB–dC35 complex, aromatic residues (Trp40, Trp54 and Phe60) on the DNA-binding surface make extensive stacking interactions with the ssDNA (13). Trp54 is located at the entrance for the 5' terminus of the ssDNA, whereas Trp40 and Phe60 function together like a clamp and located at where the 3' terminus of the ssDNA exits. Accordingly, they define the DNA-binding path and promote wrapping of the ssDNA around the homotetramer. In the PriB–dT15 structure, the L_{23} loops have a closed conformation and affect the topology of the DNA-binding surface (Figure 1C). Trp47 of monomer A, the functional equivalent of *Eco*SSB Trp54, interacts with the 3' terminus of ssDNA (Figure 2B). The clamp-like dyad (Trp40 and Phe60) found in *Eco*SSB is missing from PriB. Phe77, the functional equivalent of *Eco*SSB Phe60, is buried inside the protein. Phe42, the functional equivalent of *Eco*SSB Trp40, does not interact with DNA in the crystal structure. The 5' terminus of dT15 interacts with Trp47 of monomer B instead. Disregarding the first two bases (T1 and T2), we propose that the interaction of the dT15 5' terminus with Trp47 of monomer B directs and maximizes the interactions between the ssDNA and the OB fold of the proteins, leading the ssDNA to wrap around the L_{45} loops of the PriB dimer.

The basic residues on the PriB DNA-binding surface, with L_{45} loop in particular, play a major role in ssDNA interaction (Figure 2). Although lacking aromatic residues like Trp88 in *Eco*SSB (13), the L_{45} loop of PriB uses Lys82, Lys84 and Lys89 to make contacts with the ssDNA. These interactions were not observed in the *Eco*SSB–dC35 complex. By cooperating with Arg13 and Lys18 on the opposite side of molecules A and B' (Figures 1A and 2), Lys82, Lys84 and Lys89 stabilize nucleotides T5 to T12 by making electrostatic interactions with the sugar-phosphate backbone (Figure 2C).

The ssDNA-binding properties of PriB

The ssDNA-binding ability of PriB was estimated with filter-binding assay utilizing dA and dT oligonucleotides of various

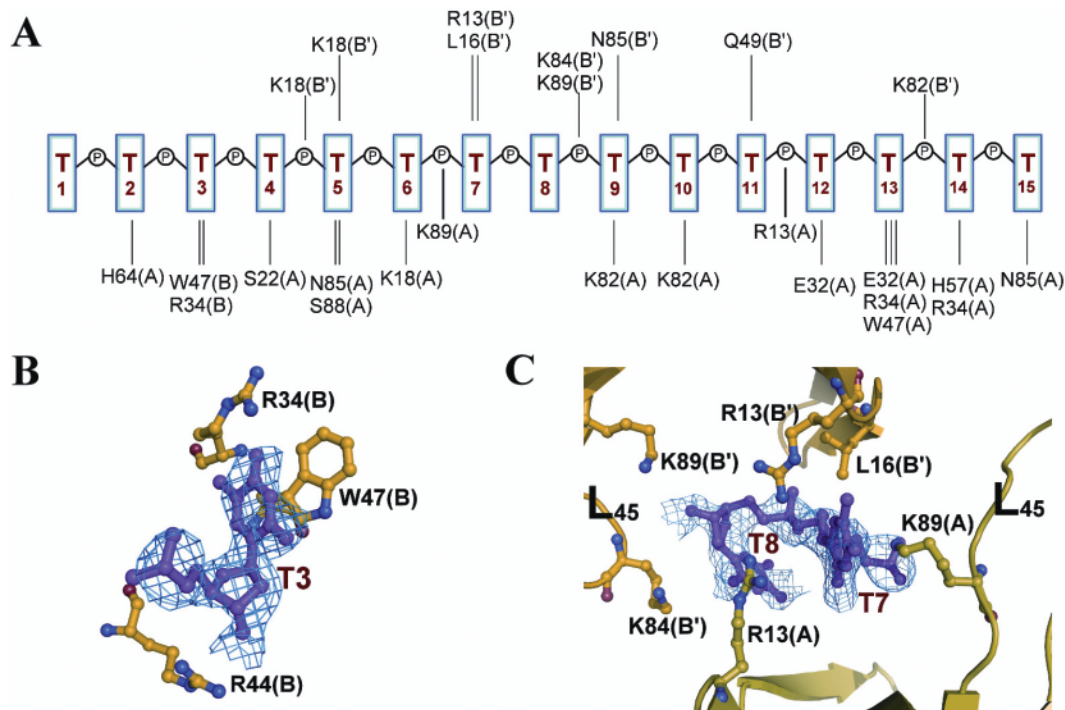


Figure 2. PriB–ssDNA interactions. (A) Schematic diagram of the protein–ssDNA interactions in the PriB–dT15 complex. The monomer that contains each amino acid is given in parentheses. (B) Stacking interactions between Trp47 and the T3 base of ssDNA. (C) Basic residues from L45 loop interact with T7 and T8 bases. The $2F_o - F_c$ electron density maps contoured at 0.8σ covering the T3 base in (B) and T7 and T8 bases in (C).

lengths. Since dT homopolymers of 20 bases or longer give high background noises upon binding to nitrocellulose filters, they were excluded from the assays. The titration curves of PriB with dA and dT homopolymers (Supplementary Figure S1) show that the affinity of PriB towards the oligonucleotides increased with length. Binding of PriB to dA5 or dT5 was negligible. Excluding dA5 or dT5, >90% of the homopolymers bound to PriB, and the estimated respective apparent K_d values are presented in Table 2. The binding affinity of PriB for ssDNA increased dramatically within a narrow range of protein concentration, indicating that the formation of PriB–ssDNA complexes is a positive cooperative process (Supplementary Figure S1). The Hill coefficients (h) for PriB–ssDNA binding were determined (Table 2). The h values for dT15, dT20, dA15, dA20 and dA25 are ~ 1.5 , suggesting cooperative binding of PriB to these homopolymers. Furthermore, a cooperativity transition occurs between dA25 and dA30, where the h values are >2.5 . The results indicate a highly cooperative binding of PriB to homopolymers of 30 bases or longer (Table 2). The cooperative binding of PriB to ssDNA has important implications for the nature of the protein–protein interactions within the complex and the position of the ssDNA-binding sites on PriB.

The ssDNA-binding surface of PriB is highly electropositive and interacts directly with both the bases and the phosphate backbone of the ssDNA. To investigate whether these electrostatic interactions play an important role in ssDNA binding, we examined the binding of ssDNA to PriB at varying salt concentrations. The binding affinity of PriB for dT15 or dA30 is salt dependent (Table 3 and Supplementary Figure S2). At 200 mM NaCl, the binding affinities of PriB

Table 2. ssDNA-binding parameters of PriB

	Apparent K_d (nM)	h
dT10	740 ± 70	1.2 ± 0.1
dT15	100 ± 20	1.5 ± 0.1
dT20	30 ± 10	1.6 ± 0.1
dA10	1280 ± 100	1.2 ± 0.1
dA15	490 ± 40	1.3 ± 0.1
dA20	290 ± 30	1.6 ± 0.1
dA25	210 ± 20	1.4 ± 0.2
dA30	120 ± 20	2.6 ± 0.2
dA35	110 ± 20	3.0 ± 0.6
dA40	70 ± 20	2.8 ± 0.5
dA45	70 ± 20	2.7 ± 0.4
dA50	40 ± 10	2.6 ± 0.4
dA55	40 ± 10	2.8 ± 0.1
dA60	40 ± 10	2.8 ± 0.2
dA65	40 ± 10	2.9 ± 0.3

The errors are standard deviations determined using 2–4 independent titration experiments.

for dT15 or dA30 are ~ 13 - and 25-fold lower than that measured in the absence of salt, respectively. Furthermore, <50% of dA30 was bound by PriB, even at micromolar concentrations of PriB (Supplementary Figure S2). These results indicate that PriB binds to ssDNA mainly through electrostatic interactions.

PriB amino acid residues crucial to ssDNA binding

To investigate the contribution of individual amino acid residues to ssDNA binding, alanine substitution and deletion mutants were constructed and analyzed (Supplementary

Table 3. Salt effect on dA30 or dT15 binding affinities of PriB

[NaCl] (mM)	dT15 $K_{d,app}$ (nM)	dA30 $K_{d,app}$ (nM)
0	100 ± 20	120 ± 20
50	170 ± 30	160 ± 30
100	300 ± 30	330 ± 30
150	560 ± 60	560 ± 60
200	1300 ± 200	3000 ± 500

The errors are standard deviations determined using 2–4 independent titration experiments.

Figure S3). Substitution at Arg13 or Lys18 had a slight effect on ssDNA binding compared to that of wild-type PriB. Interestingly, substitutions of residues in the L₄₅ loop have a greater effect on ssDNA binding. The K82A, K84A and K89A mutants have K_d values that are 4- to 6-fold (~400–600 nM) higher than that of the wild-type PriB (Table 4). Deletion of K82 or K89 (dK82 and dK89 mutants) also decreases the ssDNA-binding ability. Single mutation of positively charged residues may not sufficiently abolish the ssDNA-binding activity. A triple mutant, K82A/K84A/K89A was generated and the binding ability of this triple mutant to dT15 or dA30 impaired dramatically. The K_d for dT15 and dA30 are 5500 and 7800 nM, respectively, which are 55- to 65-fold higher than that of the wild-type PriB. These data indicate that the highly electropositive region of PriB, especially within the L₄₅ loop (which includes Lys82, Lys84 and Lys89), plays a crucial role in ssDNA binding.

Previous investigations of *EcoSSB* demonstrated that aromatic stacking plays an important role in ssDNA binding (13,27). Based on our structural data, only Trp47 of PriB is involved in ssDNA binding. To further test the relative contributions of aromatic and basic amino acids to ssDNA binding, Trp47 was point mutated. The ssDNA-binding ability of the W47A mutant is only 2.6-fold less than that of the wild-type PriB. This finding is consistent with the results of a recent report on the binding ability of the W47A mutant (as assayed using fluorescence anisotropy) (9). Hence, the aromatic residue in PriB, Trp47, appears to be involved in but not critical for ssDNA binding. Despite the presence of an *EcoSSB*-like fold in PriB, PriB appears to bind ssDNA in a different manner from *EcoSSB*.

Binding of PriB protein to circular ϕ X ssDNA

In the PriB–dT15 complex, the PriB dimers form a long chain along the ssDNA (Figure 3A and C). This arrangement is consistent with the morphology observed in negatively stained electron micrographs of PriB–circular ϕ X ssDNA complex (Figure 3B). These structural images thus reveal a novel ssDNA-binding mode that may explain how a dimeric OB-fold protein binds to ssDNA.

To examine whether the crystal structure of PriB–dT15 and the results from functional analysis of the protein with synthetic oligonucleotides are relevant to natural events, the binding of PriB protein to circular ϕ X ssDNA (5386 nt) was analyzed by agarose gel electrophoresis. By increasing the amount of PriB added, a gradual decrease in the mobility of the ϕ X ssDNA (Figure 4, lanes 1–5) can be detected. The observation probably reflects the additional copies of PriB

Table 4. ssDNA dissociation constants for PriB variants binding to dA30 or dT15

PriB variant	dT15 $K_{d,app}$ (nM)	dA30 $K_{d,app}$ (nM)
Wild-type	100 ± 20	120 ± 20
W47A	300 ± 30	310 ± 30
R13A	270 ± 30	200 ± 30
K18A	210 ± 30	210 ± 30
K82A	500 ± 50	450 ± 40
K84A	400 ± 40	420 ± 40
K89A	410 ± 40	400 ± 40
dK82	610 ± 60	550 ± 50
dK89	460 ± 50	520 ± 50
K82A/K84A/K89A	5500 ± 1000	7800 ± 1000

The errors are standard deviations determined using 2–4 independent titration experiments.

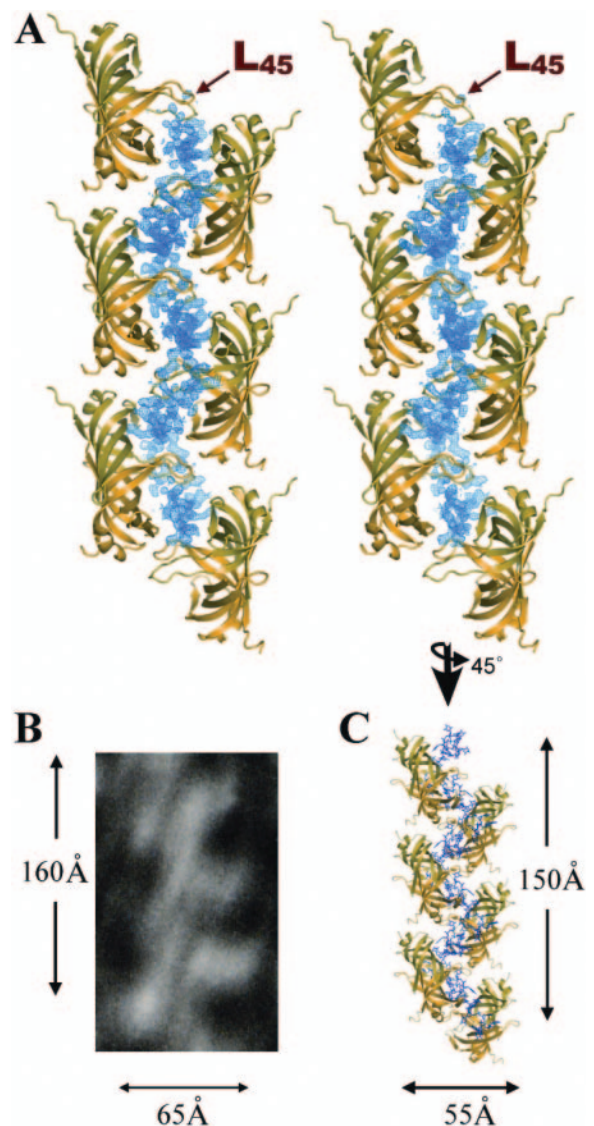


Figure 3. Topology of binding among PriB dimers and ssDNA. (A) Stereo diagram of crystal packing of PriB–dT15 complexes. The $2F_o - F_c$ electron density map contoured at 0.8σ shows the bound ssDNA (dT15) in blue. The PriB monomers are shown as green and yellow ribbons. (B) Enlarged electron micrograph of intact ϕ X ssDNA covered by PriB dimers. The arrangement of these PriB– ϕ X ssDNA complexes presented in the electron micrograph image is similar to the PriB–dT15 complexes shown in the crystal diagram in (C).

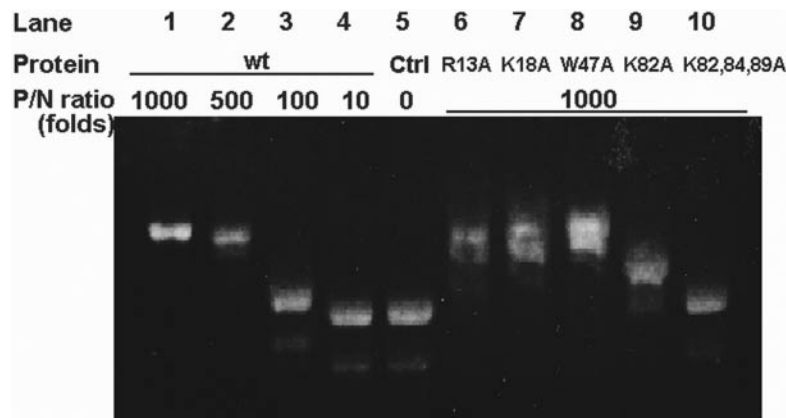


Figure 4. Binding of wild-type or PriB mutants to ϕ X ssDNA. The reaction solutions contained 100 nM circular ϕ X ssDNA and PriB proteins at the indicated protein/nucleotide concentration ratio (P/N ratio). The protein concentrations used were 100 μ M (lane 1), 50 μ M (lane 2), 10 μ M (lane 3), 1 μ M (lane 4) and without PriB protein (lane 5). The PriB mutant protein concentrations used were 100 μ M (lanes 6–10). The reaction solutions were incubated at 25°C for 30 min and then analyzed by agarose gel electrophoresis mobility shift assays. Bands correspond to unbound ϕ X ssDNA and various PriB– ϕ X ssDNA complexes were visualized by ethidium bromide staining. The minor band that is visible in the absence of PriB protein (lane 5) is contributed by a small amount of linearized ssDNA in the commercial ϕ X ssDNA preparation.

bound on to the ϕ X ssDNA and slowed down the mobility of the multicomponent complex.

Residues on PriB that are crucial to dT15 and dA30 binding are also important for ϕ X ssDNA binding. R13A, K18A or W47A mutants (Figure 4, lanes 6–8) show a minor effect while the K82A mutant has a greater effect on ϕ X ssDNA binding (Figure 4, lane 9). The mobility of the triple mutant (K82A/K84A/K89A) is nearly identical to that of the control, indicating that this protein binds ϕ X ssDNA poorly even at 1000 P/N ratios (Figure 4, lane 10).

DISCUSSION

A novel ssDNA-binding mode is revealed by the structure of the PriB–ssDNA complex

Despite the fact that both PriB and *Eco*SSB have a classical OB-fold ssDNA-binding surface (28,29), they bind DNA differentially and yield structurally distinct DNA-bound complexes. PriB dimers bind dT15 with the highly electrostatic positive L_{45} loop surface and create a long chain of protein surrounding a DNA strand (Figure 5, left panel). In contrast, a 35 nt homopolymer wraps around the *Eco*SSB tetramer in the *Eco*SSB–ssDNA complex (Figure 5, middle panel). Differences in oligomeric structure offer one apparent explanation for this observation. Moreover, the L_{23} and L_{45} loops of *Eco*SSB are longer than those of PriB. The L_{23} loop of *Eco*SSB has three aromatic residues (Trp40, Trp54 and Phe60) that are strongly involved in ssDNA binding and guide the ssDNA to wrap around the tetramer through base stacking interactions (13). The L_{23} loop of PriB also has three aromatic residues, but only Trp47 is involved in ssDNA binding. This interaction involving a single amino acid probably is insufficient to guide the ssDNA to traverse the L_{23} loop of PriB in a manner similar to that observed for *Eco*SSB. The much shorter L_{23} and L_{45} loops also preclude the possibility that PriB binds ssDNA by wrapping the DNA around a tetrameric arrangement of OB folds in a manner similar to *Eco*SSB. A large number of non-specific

DNA-binding proteins (28,29) have OB fold. Our most important finding is that PriB uses a different ssDNA-binding strategy apart from other SSBs, including human replication protein A (RPA) (Figure 5, right panel) (30). *Eco*SSB and RPA have conserved aromatic residues in the L_{45} loop of the OB fold. These residues are replaced with positively charged amino acids in PriB. These differences support our contention that the ssDNA-binding mechanisms of these OB-fold proteins might differ significantly. Indeed, our structural and functional studies reveal clear differences between the ssDNA-binding modes of these highly homologous OB-fold proteins.

Cooperative binding

Many SSB proteins bind to ssDNA with some degree of positive cooperativity. But this type of cooperativity varies considerably among the SSB proteins. For example, *Eco*SSB binds to long ssDNA in different manners that can be grouped into the (SSB)₃₅ and the (SSB)₆₅-binding modes (31). The (SSB)₃₅-binding mode has ‘unlimited’ cooperative binding while the (SSB)₆₅-binding mode promotes the ‘limited’ type of intertetramer cooperativity (31). In addition, negative cooperativity has also been observed for *Eco*SSB binding to ssDNA. The third and the fourth subunits of the SSB tetramer have reduced affinity to ssDNA (31). However, negative cooperativity has not been observed for PriB in this study, probably due to the dimeric structure of PriB and an ssDNA-binding mode that differs significantly from that of *Eco*SSB.

PriB binding to ssDNA is a positive cooperative process (Table 2). Cooperativity can result from direct protein–protein interactions between nearest neighbors, such as the LAST motif in the T4 gene 32 protein (32). Cooperativity can also result from protein-induced distortions of adjacent DNA as demonstrated by the *Sulfolobus* SSB (33). In the case of PriB, the binding activities and cooperativities are increased with longer ssDNA homopolymers (Table 2), and structural data indicate that PriB dimers cooperatively bind

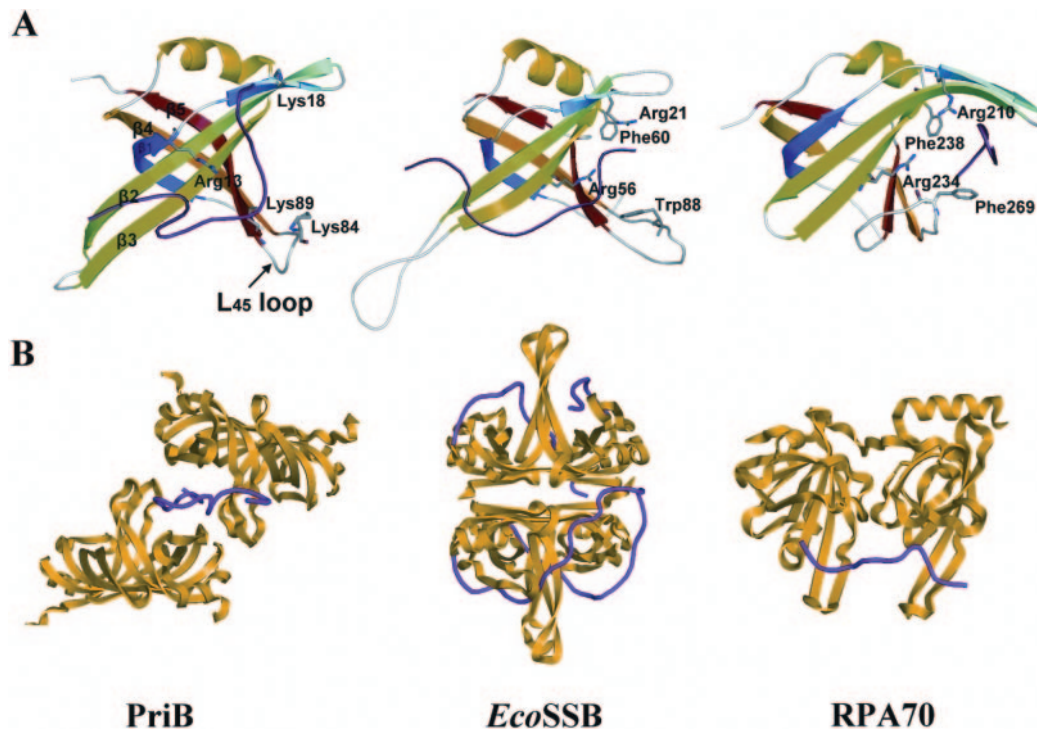


Figure 5. Ribbon diagrams of three OB-fold proteins. (A) Structural comparison of three aligned OB-fold domains: *E. coli* PriB (PDB code 2CCZ); *E. coli* SSB (PDB code 1EYG); human RPA70 (PDB code 1JMC). Residues involved in ssDNA binding are labeled. (B) Distinct ssDNA-binding modes of these OB-fold proteins. ssDNA is colored in magenta.

to the same ssDNA molecule (Figure 1B). Possibly, a PriB dimer binds and distorts the ssDNA structure. A second PriB then comes in and binds to the ssDNA. The binding of the second PriB dimer is likely the key step in forming the stable complex. Other forms of incompletely occupied PriB–ssDNA complexes may not be stable.

Binding of PriB to various ssDNA, partial duplex DNA and forked DNA is inefficient at low protein concentrations except in the presence of PriA helicase (11). Previous data also indicate that PriB can stabilize the binding of PriA to ssDNA (7). These results suggest that cooperation between PriB and PriA helicase may be necessary for PriB and/or PriA to form stable complexes with ssDNA. Interestingly, PriA has a highly electropositive ssDNA-binding region (amino acids 1–198) containing 8 Lys and 14 Arg residues (34). It might serve a role similar to monomer B' of the PriB dimer in our crystal to stabilize the partially disordered ssDNA. Possibly, PriA and PriB bind to ssDNA cooperatively, thereby decreasing the dissociation rate of PriA from the DNA during helix unwinding. Therefore, we propose that our *in vitro* assembled PriB–ssDNA complex may mimic the structure of the PriA–ssDNA–PriB complex. However, this speculation needs to be confirmed by further crystallographic study and biochemical experiments.

In conclusion, the structure of the PriB–dT15 complex and the binding properties of PriB to oligonucleotides of various lengths provide molecular details on how PriB interacts with ssDNA. Moreover, our discovery that the ssDNA-binding properties of PriB differ from that of EcoSSB suggests a basis for the distinct roles of these proteins in DNA replication.

PDB accession code

Atomic coordinates and structure factors for PriB–ssDNA complex have been deposited in the PDB under accession code 2ccz.

SUPPLEMENTARY DATA

Supplementary Data are available at NAR Online.

ACKNOWLEDGEMENTS

We thank Dr Ming F. Tam for discussion and critical reading of the manuscript. We gratefully acknowledge access to the synchrotron radiation beamline 17B2 at the National Synchrotron Radiation Research Center (NSRRC) in Taiwan. This work was supported by research grants from Academia Sinica and the National Science Council (NSC94-2311-B-001-015 to C.-D.H.), Republic of China. Funding to pay the Open Access publication charges for this article was provided by National Science Council, Taiwan, Republic of China.

Conflict of interest statement. None declared.

REFERENCES

- Cox, M.M., Goodman, M.F., Kreuzer, K.N., Sherratt, D.J., Sandler, S.J. and Marians, K.J. (2000) The importance of repairing stalled replication forks. *Nature*, **404**, 37–41.
- McGlynn, P. and Lloyd, R.G. (2002) Recombinational repair and restart of damaged replication forks. *Nature Rev. Mol. Cell Biol.*, **3**, 859–870.

3. Marians, K.J. (2000) PriA-directed replication fork restart in *Escherichia coli*. *Trends Biochem. Sci.*, **25**, 185–189.
4. Sandler, S.J. (2000) Multiple genetic pathways for restarting DNA replication forks in *Escherichia coli* K-12. *Genetics*, **155**, 487–497.
5. Sandler, S.J. and Marians, K.J. (2000) Role of PriA in replication fork reactivation in *Escherichia coli*. *J. Bacteriol.*, **182**, 9–13.
6. Heller, R.C. and Marians, K.J. (2005) The disposition of nascent strands at stalled replication forks dictates the pathway of replisome loading during restart. *Mol. Cell*, **17**, 733–743.
7. Liu, J., Nurse, P. and Marians, K.J. (1996) The ordered assembly of the ϕ X174-type primosome. III. PriB facilitates complex formation between PriA and DnaT. *J. Biol. Chem.*, **271**, 15656–15661.
8. Liu, J.H., Chang, T.W., Huang, C.Y., Chen, S.U., Wu, H.N., Chang, M.C. and Hsiao, C.D. (2004) Crystal structure of PriB, a primosomal DNA replication protein of *Escherichia coli*. *J. Biol. Chem.*, **279**, 50465–50471.
9. Lopper, M., Holton, J.M. and Keck, J.L. (2004) Crystal structure of PriB, a component of the *Escherichia coli* replication restart primosome. *Structure*, **12**, 1967–1975.
10. Shioi, S., Ose, T., Maenaka, K., Shiroishi, M., Abe, Y., Kohda, D., Katayama, T. and Ueda, T. (2005) Crystal structure of a biologically functional form of PriB from *Escherichia coli* reveals a potential single-stranded DNA-binding site. *Biochem. Biophys. Res. Commun.*, **326**, 766–776.
11. Cadman, C.J., Lopper, M., Moon, P.B., Keck, J.L. and McGlynn, P. (2005) PriB stimulates PriA helicase via an interaction with single-stranded DNA. *J. Biol. Chem.*, **280**, 39693–39700.
12. Chase, J.W. and Williams, K.R. (1986) Single-stranded DNA binding proteins required for DNA replication. *Annu. Rev. Biochem.*, **55**, 103–136.
13. Raghunathan, S., Kozlov, A.G., Lohman, T.M. and Waksman, G. (2000) Structure of the DNA binding domain of *E. coli* SSB bound to ssDNA. *Nature Struct. Biol.*, **7**, 648–652.
14. Wang, C.C., Chang, T.C., Lin, C.W., Tsui, H.L., Chu, P.B., Chen, B.S., Huang, Z.S. and Wu, H.N. (2003) Nucleic acid binding properties of the nucleic acid chaperone domain of hepatitis delta antigen. *Nucleic Acids Res.*, **31**, 6481–6492.
15. Wong, I. and Lohman, T.M. (1993) A double-filter method for nitrocellulose-filter binding: application to protein–nucleic acid interactions. *Proc. Natl Acad. Sci. USA*, **90**, 5428–5432.
16. Abbani, M., Iwahara, M. and Clubb, R.T. (2005) The structure of the excisionase (Xis) protein from conjugative transposon Tn916 provides insights into the regulation of heterobivalent tyrosine recombinases. *J. Mol. Biol.*, **347**, 11–25.
17. Grove, D.E., Willcox, S., Griffith, J.D. and Bryant, F.R. (2005) Differential single-stranded DNA binding properties of the paralogous SsbA and SsbB proteins from *Streptococcus pneumoniae*. *J. Biol. Chem.*, **280**, 11067–11073.
18. Otwinowski, Z. and Minor, W. (1997) Processing of X-ray diffraction data collected in oscillation mode. *Methods Enzymol.*, **276**, 307–326.
19. Navaza, J. (1994) AMoRe: an automated package for molecular replacement. *Acta Crystallogr.*, **D50**, 157–163.
20. McRee, D.E. (1999) XtalView/Xfit—a versatile program for manipulating atomic coordinates and electron density. *J. Struct. Biol.*, **125**, 156–165.
21. Read, R.J. (1986) Improved Fourier coefficients for maps using phases from partial structures with errors. *Acta Crystallogr.*, **A42**, 140–149.
22. Brünger, A.T., Adams, P.D., Clore, G.M., DeLano, W.L., Gros, P., Grosse-Kunstleve, R.W., Jiang, J.S., Kuszewski, J., Nilges, M., Pannu, N.S. *et al.* (1998) Crystallography and NMR system: a new software suite for macromolecular structure determination. *Acta Crystallogr.*, **D54**, 905–921.
23. Laskowski, R.A., MacArthur, M.W., Moss, D.S. and Thornton, J.M. (1993) PROCHECK: a program to check the stereochemical quality of protein structures. *J. Appl. Crystallogr.*, **26**, 283–291.
24. Shamo, Y., Friedman, A.M., Parsons, M.R., Konigsberg, W.H. and Steitz, T.A. (1995) Crystal structure of a replication fork single-stranded DNA binding protein (T4 gp32) complexed to DNA. *Nature*, **376**, 362–366.
25. Romer, R., Schomburg, U., Krauss, G. and Maass, G. (1984) *Escherichia coli* single-stranded DNA binding protein is mobile on DNA: ¹H NMR study of its interaction with oligo- and polynucleotides. *Biochemistry*, **23**, 6132–6137.
26. Ponomarev, V.A., Makarova, K.S., Aravind, L. and Koonin, E.V. (2003) Gene duplication with displacement and rearrangement: origin of the bacterial replication protein PriB from the single-stranded DNA-binding protein Ssb. *J. Mol. Microbiol. Biotechnol.*, **5**, 225–229.
27. Raghunathan, S., Ricard, C.S., Lohman, T.M. and Waksman, G. (1997) Crystal structure of the homo-tetrameric DNA binding domain of *Escherichia coli* single-stranded DNA-binding protein determined by multiwavelength x-ray diffraction on the selenomethionyl protein at 2.9-Å resolution. *Proc. Natl Acad. Sci. USA*, **94**, 6652–6657.
28. Theobald, D.L., Mitton-Fry, R.M. and Wuttke, D.S. (2003) Nucleic acid recognition by OB-fold proteins. *Annu. Rev. Biophys. Biomol. Struct.*, **32**, 115–133.
29. Murzin, A.G. (1993) OB(oligonucleotide/oligosaccharide binding)-fold: common structural and functional solution for non-homologous sequences. *EMBO J.*, **12**, 861–867.
30. Bochkarev, A., Pfuetzner, R.A., Edwards, A.M. and Frappier, L. (1997) Structure of the single-stranded-DNA-binding domain of replication protein A bound to DNA. *Nature*, **385**, 176–181.
31. Lohman, T.M. and Ferrari, M.E. (1994) *Escherichia coli* single-stranded DNA-binding protein: multiple DNA-binding modes and cooperativities. *Annu. Rev. Biochem.*, **63**, 527–570.
32. Casas-Finet, J.R., Fischer, K.R. and Karpel, R.L. (1992) Structural basis for the nucleic acid binding cooperativity of bacteriophage T4 gene 32 protein: the (Lys/Arg)³(Ser/Thr)² (LAST) motif. *Proc. Natl Acad. Sci. USA*, **89**, 1050–1054.
33. Kerr, I.D., Wadsworth, R.I., Cubeddu, L., Blankenfeldt, W., Naismith, J.H. and White, M.F. (2003) Insights into ssDNA recognition by the OB fold from a structural and thermodynamic study of Sulfolobus SSB protein. *EMBO J.*, **22**, 2561–2570.
34. Chen, H.W., North, S.H. and Nakai, H. (2004) Properties of the PriA helicase domain and its role in binding PriA to specific DNA structures. *J. Biol. Chem.*, **279**, 38503–38512.